Density Functional Theory for Planar Electric Double Layers: Closing the Gap between Simple and Polyelectrolytes

Zhidong Li and Jianzhong Wu*

Department of Chemical and Environmental Engineering, University of California, Riverside, California 92521-0425

Received: January 7, 2006; In Final Form: February 17, 2006

We report a nonlocal density functional theory (NLDFT) for polyelectrolyte solutions within the primitive model; i.e., the solvent is represented by a continuous dielectric medium, and the small ions and polyions by single and tangentially connected charged hard spheres, respectively. The excess Helmholtz energy functional is derived from a modified fundamental measure theory for hard-sphere repulsion, an extended first-order thermodynamic perturbation theory for chain connectivity, and a quadratic functional Taylor expansion for electrostatic correlations. With the direct and cavity correlation functions of the corresponding monomeric systems as inputs, the NLDFT predicts the segment-level microscopic structures and adsorption isotherms of polyelectrolytes at oppositely charged surfaces in good agreement with molecular simulations. In particular, it faithfully reproduces the layering structures of polyions, charge inversion, and overcharging that cannot be captured by alternative methods including the polyelectrolyte Poisson−Boltzmann equation and an earlier version of DFT. The NLDFT has also been used to investigate the influences of the small ion valence, polyion chain length, and size disparity between polyion segments and counterions on the microscopic structure, mean electrostatic potential, and overcharging in planar electric double layers containing polyelectrolytes.

I. Introduction

Electrolyte solutions are ubiquitous in nature and in industrial processes and have been subjected to a long history of fundamental research.[1,2] However, a molecular-level understanding of the microscopic structure and thermophysical properties of electrolyte solutions remains incomplete not only because of the cryptic nature of water as the prime solvent but also because of the multibody correlations induced by long-range Coulomb interactions that make typical mean-field methods ineffectual. The task is more challenging for systems containing charged polymers or polyelectrolytes in which theoretical modeling is further complicated by chain connectivity.[3,4] From a practical point of view, conventional theories of electrolyte solutions are primarily based on various analytical solutions to the Poisson−Boltzmann (PB) equation that juxtaposes classical electrostatics with Boltzmann's distribution for mobile charges. These include the Gouy−Chapman (GC) theory for inhomogeneous distributions of small ions near charged subjects[5,6] or the Debye−Hückel (DH) theory for bulk electrolyte solutions.[7] Numerous semiempirical modifications of GC or DH theory have been proposed by considering the chemical nature of ionic species[8−12] and/or physical characteristics such as ion size, valence, and electrostatic correlations.[13−20] Advanced statistical−mechanical theories are now available to truthfully incorporate the excluded-volume effects and electrostatic/density correlations within the primitive model wherein the solvent is represented by a dielectric continuum. For solutions containing polyelectrolytes, on the other hand, early theoretical investigations were primarily based on the cell model where polyions are represented by rigid rods and the ionic distributions are described either by the cylindrical PB equation or by incorporation of the concept of counterion condensation.[21,22] Although the cell model ignores polymer conformations completely, it predicts various macroscopic properties of natural and synthetic polyelectrolyte solutions in good agreement with experiments. Indeed, the cell model provides a simple yet effectual way to describe the osmotic pressures of DNA and polyelectrolyte solutions,[21] mean-activity coefficients,[23] ζ-potentials, potentiometer titration and ion binding,[24] salt-induced chromatin condensation,[25] and thermodynamic stability of double-strand DNA structures.[26,27] Conversely, more recent theoretical developments on polyelectrolyte solutions are primarily based on scaling analysis,[28,29] polymer-field theory,[30−35] polyelectrolyte Poisson−Boltzmann approximation,[36] and integral-equation theories.[37−39] These more recent investigations are mainly concerned with polymer configurations or inter- and intramolecular correlation functions of polyions. In comparison with the cell model, the more sophisticated theories retain the chain flexibility of polyelectrolytes and provide deeper insights into the solution microscopic structure. However, their broad applications, to strongly charged inhomogeneous systems in particular, are often limited by difficulties in appropriate incorporation of charge fluctuations or in the selection of reliable closures to attain a self-consistent description of both intra- and intermolecular correlation functions.

As a generic methodology in statistical mechanics, density functional theory (DFT) offers a powerful alternative to conventional mean-field methods including the PB equation and integral-equation theories for simple and polyelectrolytes.[40,41] Indeed, many conventional mean-field methods can be reformulated in the framework of DFT at different levels of approximation. DFT is applicable to both coarse-grained and atomistic models, and its numerical performance can be directly tested with molecular simulation. Moreover, the numerical efficiency of DFT makes it an ideal choice for systems with multiple length scales beyond the scope of conventional

* E-mail: jwu@engr.ucr.edu.

10.1021/jp060127w CCC: $33.50
Published on Web 03/17/2006

molecular simulations. Applications of DFT to simple electrolyte solutions, electric double layers, and colloidal forces have been extensively reported.[42−48] With an appropriate expression of the excess free-energy functional accounting for various components of intermolecular forces, DFT has been successfully used to describe interesting electrostatic phenomena such as attraction between like charged surfaces and charge inversion that cannot be captured by the PB-based methods. It has also been applied to colloidal dispersions and concentrated solutions of macroions and neutral particles mimicking crowded cellular environments.[49−51] Whereas DFT has long been recognized as a promising theoretical approach to modeling polymeric systems, relatively few studies have been reported on its application to polyelectrolytes.[52,53]

In our previous publications,[54−58] we have used DFT to study the structure and thermodynamic properties of highly asymmetric electrolyte solutions and electric double layers of different geometry. With the excluded-volume effects described by a modified fundamental measure theory[59,60] and the long-range Coulomb correlations represented by a quadratic expansion of the excess Helmholtz energy functional, we demonstrated that DFT is able to describe the ionic distributions, correlation functions, and ζ-potentials of charged surfaces in quantitative agreement with molecular simulations. For systems containing monovalent ions, the numerical performance of the DFT is comparable to that of integral-equation theories and of the modified PB equation. For systems containing multivalent ions, however, DFT can be substantially more accurate than alternative methods.[47,56,61−64] In this work, we extend the formulism of the excess Helmholtz energy functional for simple electrolyte solutions to that for linear polyelectrolytes by using a thermodynamic perturbation theory (TPT) for inhomogeneous polymeric fluids.[65,66] Being consistent with the primitive model for electrolyte solutions, we use a simple model of polyelectrolytes wherein small ions and segments of tangentially connected polyions are represented by charged spheres and the solvent is represented by a dielectric continuum. A similar polyelectrolyte model was recently used by Yethiraj and co-workers, and their simulation results for relatively short polyelectrolyte chains near oppositely charged surfaces provide a direct test of the present version of DFT.[52,67]

The remainder of this article is organized as follows. Section II describes the model systems and formulation of the Helmholtz energy functional for polyelectrolyte solutions. Section III discusses the numerical performance of the theory by direct comparison with the simulation results for the local density distributions and surface excesses of short-chain polyelectrolytes near an oppositely charged surface. Next, we discuss applications of DFT to adsorption of long-chain polyelectrolytes concerned with the influences of the ion size and valence. In section III, we also investigate the effect of the polyion chain length on the mean electrostatic potential and integrated charge distribution function near an oppositely charged surface. Because DFT is directly applicable to simple as well as polyelectrolytes within the same theoretical framework, attention is also given to variations of the electrostatic potential and microscopic structures of planar electric double layers when the source of mobile charges changes from simple ions to long polyelectrolytes. Section IV summarizes the main results and conclusions. A brief account of this work has been reported elsewhere.[68]

II. Molecular Model and Theory

We consider a primitive model of polyelectrolyte solutions where the polymers are represented by tangentially jointed chains of charged hard spheres, small ions are monomeric charged hard spheres, and the solvent is a continuous dielectric medium. The polymer segments are indistinguishable (homopolymer) but are not necessarily the same as the small ions. The reduced interaction potential between any pair of charged spheres is given by

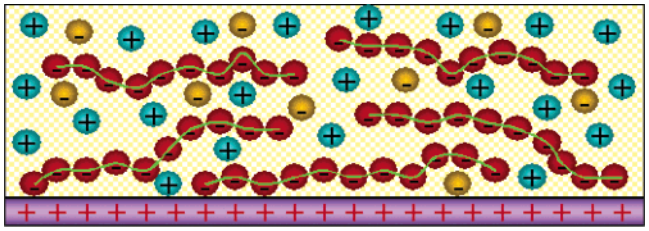

Figure 1. Schematic diagram of the electric double layer model for polyelectrolyte solutions.

$$\beta u_{ij}(r) = \begin{cases} \infty & r < \sigma_{ij} \\ l_B \dfrac{Z_i Z_j}{r} & r \geq \sigma_{ij} \end{cases} \tag{1}$$

where r is the center-to-center distance, σ_k is the sphere diameter with $\sigma_{ij} = (\sigma_i + \sigma_j)/2$, Z_k is the valence, and $l_B = \beta e^2/\epsilon$ is the Bjerrum length that represents the separation between two unit charges (e) in a dielectric medium of relative permittivity ϵ such that the electrostatic potential is equal to the thermal energy k_BT. In an aqueous solution at 298 K, $l_B = 0.714$ nm. As for freely jointed tangent hard-sphere chains, the bonding potential $V_b(\mathbf{R})$ for a polyion is determined from

$$\exp[-\beta V_b(\mathbf{R})] = \prod_{i=1}^{M-1} \frac{\delta(|\mathbf{r}_{i+1} - \mathbf{r}_i| - \sigma_p)}{4\pi\sigma_p^2} \tag{2}$$

where M stands for the degree of polymerization, $\mathbf{R} \equiv (\mathbf{r}_1, \mathbf{r}_2, ..., \mathbf{r}_M)$ is a set of coordinates specifying the segmental positions or polymer configuration, and δ is the Dirac-delta function. The subscripts "p", "+", and "−" denote polyion segments, cations, and anions, respectively.

Near a uniformly charged planar surface, the external potential for each charged sphere (a polymer segment or a small ion) is given by

$$\beta\Psi_k(z) = \begin{cases} \infty & z < \sigma_k \\ -2\pi l_B Z_k z \dfrac{Q}{e} & z \geq \sigma_k \end{cases} \tag{3}$$

where Q denotes the surface charge density and z is the perpendicular distance from the surface. Figure 1 shows a schematic diagram of the electric double layer model where the polyelectrolyte solution is in contact with a uniformly charged planar surface.

Whereas DFT provides an exact mathematical framework for the realization of statistical thermodynamics, its performance entirely depends on the formulation of the grand potential Ω, or equivalently, of the Helmholtz energy functional F in terms of the molecular density profiles. The central task for the application of DFT is therefore to derive an analytical expression of the Helmholtz energy as a functional of the underlying density profiles. In general, the Helmholtz energy functional can be formally expressed as the sum of an ideal-gas term, F^{id}, that preserves the bond connectivity and an excess, F^{ex}, that takes into account all nonbonded interactions. While the ideal-gas Helmholtz energy is known exactly by using either the polymer-field theory for a continuous model of chain connectivity[30] or

simply multidimensional integrations for an explicit model of bond potentials,[36] the excess Helmholtz energy arising from nonbonded interactions, i.e., hard-sphere repulsion and Coulomb interactions in the primitive model of polyelectrolytes, can only be formulated at various levels of mean-field approximations. These approximations may differ substantially not only in terms of numerical accuracy but also in the qualitative deliberation of the underlying physics. The particular version of DFT used in this work accounts for the contributions to the Helmholtz energy from multibody correlations by using a modified fundamental measure theory (FMT) for hard-sphere repulsions,[59,60] a quadratic functional expansion (or hypernetted-chain approximation, HNC) for the electrostatic interactions,[57,69] and the first-order thermodynamic perturbation theory (TPT1) for intrachain connectivity.[66,70] Similar expressions of the free-energy functionals have been used in our previous work for confined associating fluids,[71] polymeric fluids,[66,70] and electrolyte solutions.[54,57] A complete neglect of the size effects and correlations in our DFT would reduce the Helmholtz energy to that used in the polyelectrolyte Poisson−Boltzmann (PPB) approximation[36] or equivalently, in terms of the continuous Gaussian model for the chain connectivity, to that used in the self-consistent-field theory for polyelectrolytes.[30] The appendix provides the detailed expressions of the Helmholtz energy functional used in this work.

Minimization of the grand potential yields the Euler−Lagrange equations for the density profiles of the polyions and small ions:

$$\rho_M(\mathbf{R}) = \exp\left\{\beta\mu_M - \beta V_b(\mathbf{R}) - \sum_{i=1}^{M}\left[\beta\Psi_p(\mathbf{r}_i) + \frac{\delta\beta F^{ex}}{\delta\rho_p(\mathbf{r}_i)}\right]\right\} \quad (4)$$

$$\rho_\alpha(\mathbf{r}) = \exp\left[\beta\mu_\alpha - \beta\Psi_\alpha(\mathbf{r}) - \frac{\delta\beta F^{ex}}{\delta\rho_\alpha(\mathbf{r})}\right] \quad (5)$$

For a homopolymer consisting of M identical segments, the overall segment density can be determined from

$$\rho_p(\mathbf{r}) = \sum_{i=1}^{M}\rho_{si}(\mathbf{r}) = \sum_{i=1}^{M}\int d\mathbf{R}\,\delta(\mathbf{r}-\mathbf{r}_i)\rho_M(\mathbf{R}) \quad (6)$$

For more efficient numerical computation of the density profiles of charged species, we define the mean electrostatic potential

$$Z_k e\psi(\mathbf{r}) = \Psi_k^C(\mathbf{r}) + \frac{\delta F_C^{ex}}{\delta\rho_k(\mathbf{r})} \quad (7)$$

where the first term on the right-hand side is the electrostatic potential due to the surface charge and the second terms arises from the interactions among mobile charges. This mean electrostatic potential is the same as that used in the PB equation. The electrostatic potential and subsequently the density profiles of polymer segments and small ions are solved using the Picard iteration method. The numerical details for solving the density profiles are discussed in the Appendix.

III. Results and Discussion

A. Numerical Test. We test the numerical performance of the DFT by direct comparison with Monte Carlo simulations for the distributions of small ions and polyions near an oppositely charged surface. In the simulations,[52,67] each polyion consisted of $M = 10$ negatively charged segments ($Z_p = -1$) and all small ions were monovalent ($Z_+ = -Z_- = 1$). The diameters of polyion segments (σ_p) and small ions (σ_+ and σ_-) were assumed the same as the Bjerrum length. The polyelectrolyte solutions in the bulk were at nearly salt-free conditions; i.e., the concentration of coions in the bulk was so small that its influence on polyion distributions was essentially negligible.

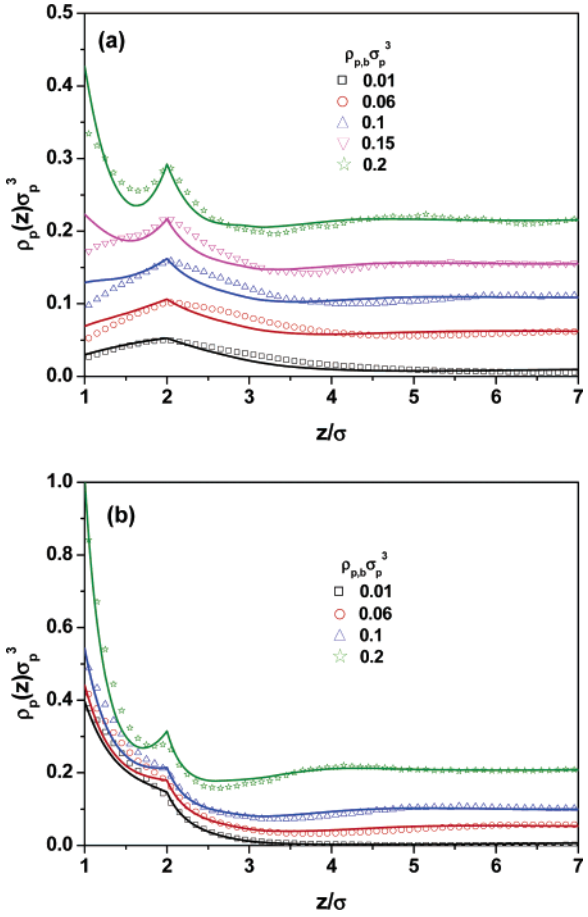

Figure 2. Density profiles of polyion segments near an oppositely charged surface with the surface charge density (a) $Q\sigma^2/e = 0.0625$ and (b) $Q\sigma^2/e = 0.25$. The polyion segments and small ions have the same size and valence, i.e., $\sigma_p = \sigma_+ = \sigma_- = \sigma = 0.714$ nm and $Z_p = -Z_+ = Z_- = -1$, and the polyion chain length is $M = 10$. The lines are predictions of DFT, and the symbols are simulation results from refs 52 and 67.

Figures 2 and 3 present, respectively, the density profiles of polyion segments and of counterions (i.e., those ions with a charge opposite to polyions) near a uniformly charged surface at two reduced charge densities, $Q\sigma^2/e = 0.0625$ and 0.25. The lines are predicted by the DFT, and the symbols are from molecular simulations. Figure 2a shows the density profiles of the polyion near a weakly charged surface ($Q\sigma^2/e = 0.0625$) as the reduced density in the bulk increases from $\rho_{p,b}\sigma_p^3 = 0.01$ to 0.2. While the polyions are in general accumulated near the surface due to the direct electrostatic attraction, a weak depletion, similar to that observed for neutral polymers, is also evident. As in the adsorption of neutral polymers,[66] the depletion is introduced by the restriction of polyion configurations near the surface and the "kink" at $z = 2\sigma$ arises from the Dirac-delta function used for representing the bonding potential. Because of the excluded-volume effects, the surface depletion disappears as the polyion concentration increases and a layering effect is observed at high polyion density. Away from the weakly charged surface, the segment density of polyions exhibits an

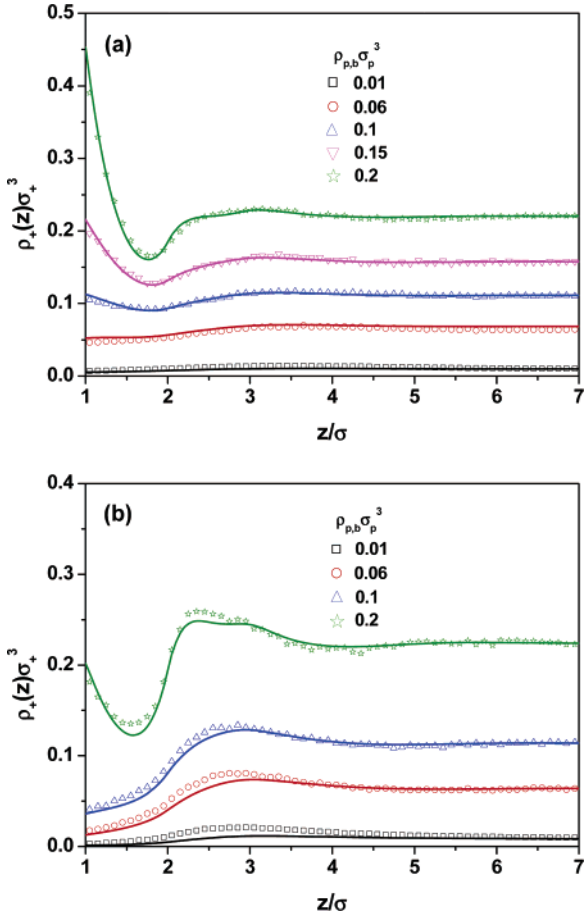

Figure 3. Same as Figure 2 but for the density profiles of counterions.

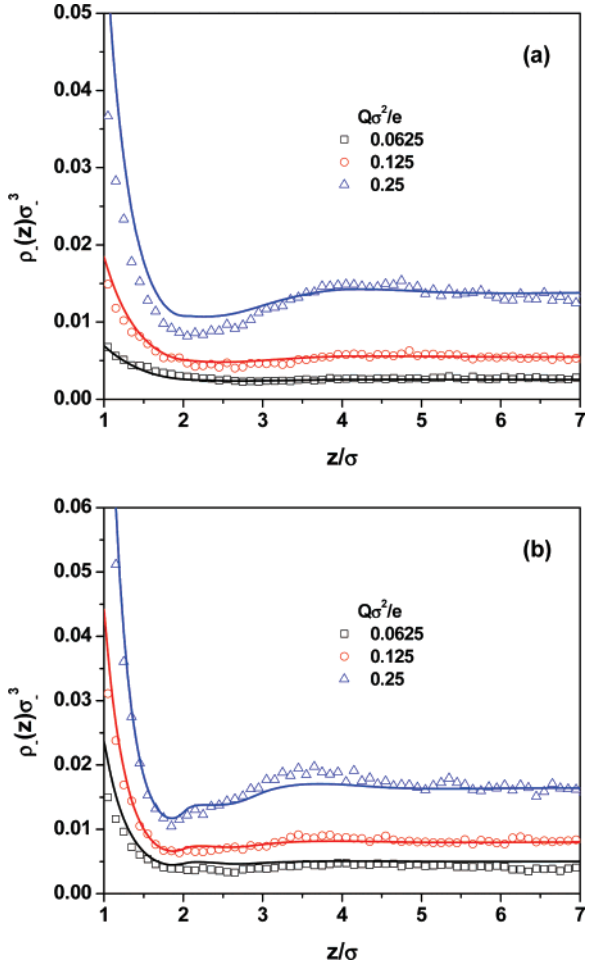

Figure 4. Density profiles of coions at (a) $\rho_{p,b}\sigma_p^3 = 0.1$ and (b) $\rho_{p,b}\sigma_p^3 = 0.2$. All the parameters are the same as those in Figure 2.

oscillatory behavior due to the long-range correlations introduced by the Coulomb interactions and by the chain connectivity. Near the surface of higher charge density (Figure 2b, $Q\sigma^2/e = 0.25$), the direct Coulomb attraction from the surface results in a stronger adsorption of polyions. In this case, the entropy-induced surface depletion and long-range oscillation of the polyion density become less distinctive, suggesting a suppression of the effects of both chain connectivity and long-range electrostatic correlations. Because of the charge localization, the density profiles of polyion segments exhibit pronounced local excluded-volume effects as evidence in the layering structure around $z/\sigma = 2$.

Figure 3 presents the density distributions of the counterions corresponding to those systems shown in Figure 2. Near the weakly charged surface, the distribution of counterions is essentially uniform at low polyion concentration, but at high polyion concentration, an accumulation of counterions is observed due to the adsorption of polyions and the excluded-volume effects. At the surface of higher charge density ($Q\sigma^2/e = 0.25$), the counterion density is significantly lower than the bulk density owing to the enhanced electrostatic repulsion from the surface. In Figure 4, we compare the theoretical density profiles of coions with the simulation data.

Figures 2−4 indicate that the density distributions of polyions and small ions predicted by the DFT are in good agreement with Monte Carlo simulations. In particular, the DFT faithfully reproduces the long-range oscillations and layering structure. Nevertheless, near a weakly charged surface, the DFT predicts the contact polyion densities systematically higher than the simulation results. By examining the distributions of small ions, we suspect that this deficiency is probably due to the approximations introduced in the first-order thermodynamic perturbation theory for the chain connectivity. The accumulation of polyelectrolytes at an oppositely charged surface is strengthened by the excluded-volume effects and electrostatic correlations. In contrast, chain connectivity weakens this accumulation. As for bulk polymeric fluids, TPT1 ignores the correlations beyond the nearest neighbors and thereby underestimates the effect of chain connectivity. That explains why the current version of DFT slightly overpredicts the contact densities of polyions.

Figure 5 shows variations of the mean electrostatic potential for those systems considered in Figures 2−4. Unlike the predictions based on the PB equation[36] or a polymer mean-field theory,[30] the mean electrostatic potential near a positively charged surface does not monotonically decline to zero. Instead, it falls rapidly near the surface (approximately within $z/\sigma < 2$) and reaches a negative minimum even though the bare surface carries positive charges. The negative sign indicates that near the charged surface, the overall electrostatic potential (due to both the surface and mobile charges) becomes opposite to that due to the bare surface. This charge inversion phenomenon is not captured by the PB equation or by an early version of DFT.[52] At a fixed surface charge density, an increase of the bulk concentration leads to a higher contact density of polyions (as shown in Figure 2) and a reduction of the contact electrostatic potential. The increased bulk concentration also results in stronger excluded-volume effects that shift the position of the minimum electrostatic potential closer to the surface. Interestingly, the absolute value of the minimum electrostatic potential

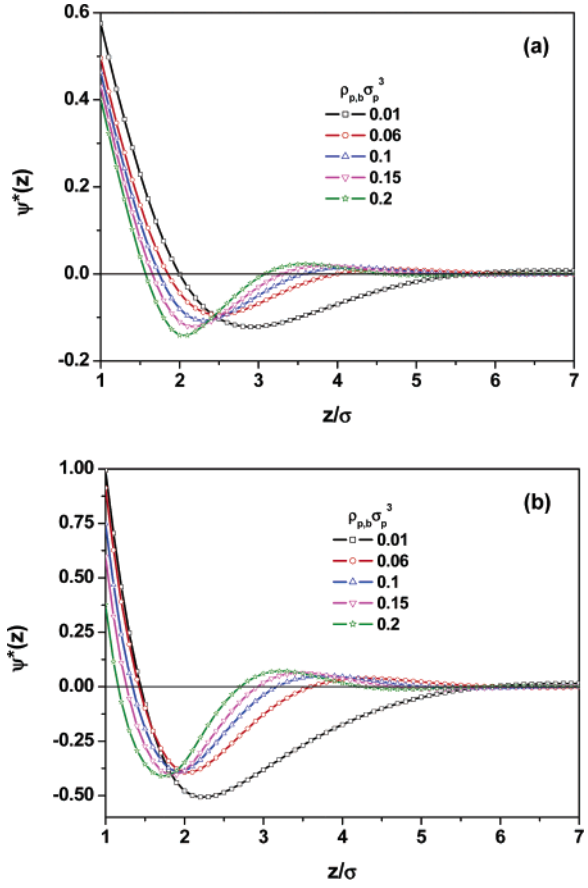

Figure 5. Mean electrostatic potentials predicted by the DFT. All parameter are the same as those used in Figure 2.

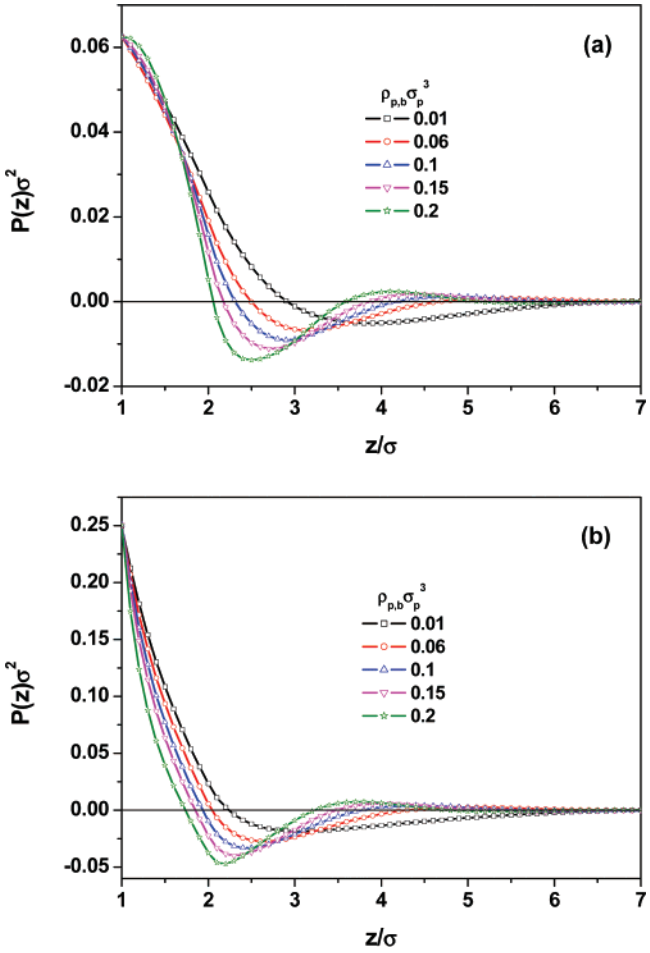

Figure 6. Integrated charge distribution functions predicted by the DFT. All parameter are the same as those used in Figure 2.

first decreases with the polyion concentration and then the trend is reversed as the polyion concentration is further increased. The nonmonotonic effect of the polyion density on the mean electrostatic potential can be explained by considering different contributions to the polyion distributions, namely, charge correlations and excluded-volume effects that are responsible for charge inversion at low and high polyion concentrations, respectively. A comparison of Figure 5a and b suggests that, qualitatively, the distribution of electrostatic potential varies little with the surface charge density. Nevertheless, Figure 5b shows that, at the same polyion concentration, charge inversion becomes more pronounced as the surface charge density increases.

The charge inversion is also manifested in the integrated charge distribution function that describes an overall charge near the surface

$$P(z) = \int_0^z dz' \sum_{k=p,+,-} Z_k \rho_k(z') + \frac{Q}{e} \qquad (8)$$

Within contact ($z \leq \sigma$), $P(z)$ is defined by the surface charge density Q/e, and for $z > \sigma$, it includes contributions from the charged surface and those from polyions and small ions. The integrated charge distribution function is related to the mean-electrostatic potential by $d\psi^*(z)/dz = -4\pi l_B P(z)$. Figure 6 shows that the integrated charge distribution function exhibits a negative minimum near the surface, suggesting an over adsorption of the negatively charged polyions. The magnitude of the overcompensated charge monotonically increases with the polyion concentration, and the position at the minimum value of the integrated charge, which is slightly larger than that at the minimum electrostatic potential, shifts closer to the surface. As the surface charge density increases, the overcharging becomes more prominent. An early version of DFT[52] fails to describe the overcharging because in order to capture the layering structure of polyions near the surface, we need to have accurate expressions of the Helmholtz energy functional not only for the long-range Coulomb interactions but also for the chain connectivity and segment-level excluded-volume effects.

Macroscopically, the adsorption of polyelectrolytes is described by the surface excess

$$\Gamma_{ex} = \int_{\sigma_p}^{\infty} [\rho_p(z) - \rho_{p,b}]\, dz \qquad (9)$$

Figure 7 shows a comparison between the DFT and Monte Carlo simulations for the surface excesses of polyions near oppositely charged surfaces. As expected, more polyions are adsorbed as the surface charge density increases. Less intuitive though is that, unlike the Langmuir adsorption isotherms, the surface excess displays a nonmonotonic variation with respect to the bulk polyelectrolyte concentration. The adsorption isotherm exhibits a concave shape with a shallow minimum at a moderate polyelectrolyte concentration. As the surface charge density increases, this minimum slowly moves in the direction of a higher polyelectrolyte concentration. The reduction of surface excess with the bulk concentration can be explained by the restriction of chain configuration and by the charge inversion that occurs even at very low polyion concentrations, and the weak increase of adsorption at high polyion density is attributed to the excluded-volume effects. In the former case, the

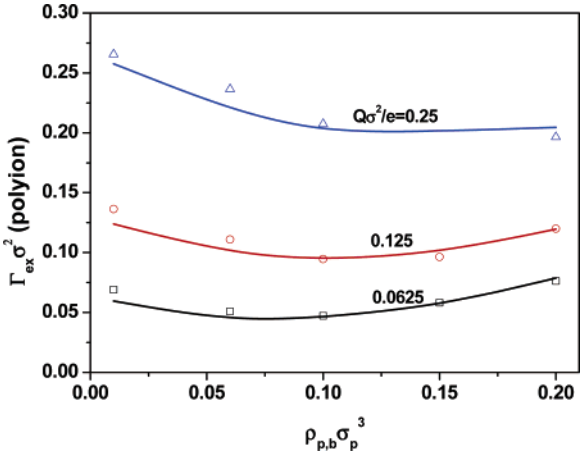

Figure 7. Adsorption isotherms of polyions at different surface charge densities $Q\sigma^2/e = 0.0625$, 0.125, and 0.25. As in Figure 2, the lines are theoretical predictions and the symbols are simulation results from ref 52.

overcharging effects become stronger as the concentration increases and thereby prevent the further adsorption of similarly charged polyions. Conversely, the excluded-volume effects overrule the overcharging when the concentration is sufficiently high. In that case, the accumulation of polyions near the surface is enhanced as the polyion concentration increases.

B. Effects of Counterion Valence and Size Disparity. Different from alternative theories of polyelectrolyte solutions, DFT accounts for the size and valence of polyion segments and counterions explicitly. We expect that these parameters may play an important role in systems involving strong electrostatic interactions where conventional mean-field methods become inadequate. To investigate the effects of ion valence and size on polyelectrolyte adsorption, we consider again the polyion segment distributions near an oppositely charged surface within the primitive model. However, more realistic parameters are now used for both the polyelectrolyte chain length and ion diameter. The diameter of counterions σ_+ is chosen at 0.425 nm, which is more reasonable for simple inorganic ions. The polyelectrolyte concentration in the bulk and the surface charge density are fixed at $\rho_{p,b}\sigma_p^3 = 0.1$ and $Q\sigma^2/e = 0.175$, respectively. All polyelectrolyte systems are under salt-free conditions; i.e., there are no coions in the bulk solution.

Figure 8a shows the distributions of polyion segments and of counterions at three counterion valences. As before, each polyion segment bears one negative charge and its diameter is the same as that of the small ions; i.e., $Z_p = -1$ and $\sigma_p = 0.425$ nm. However, here, the polyion chain length is $M = 100$, significantly longer than that used in the Monte Carlo simulations. As the counterion valence increases from $Z_+ = 1$ to 3, we see little variation in the density profiles of polyions, indicating that polyelectrolyte adsorption is mainly determined by the direct electrostatic attraction from the surface. In addition, the segmental density profiles show no long-range correlations in the direction perpendicular to the surface even though the chain length is substantially increased. In other words, for polyions near an oppositely charged surface, the correlations due to chain connectivity and Coulomb interactions are substantially abated. In all cases, the segment density profiles show prominent oscillations in the vicinity of the surface because of the chain connectivity and the segment-level excluded-volume effects introduced by the strong localization of polyions. Counterions are depleted from the surface due to the direct electrostatic repulsion, and the depletion is magnified as the valence increases. The accumulation of counterions around 3σ

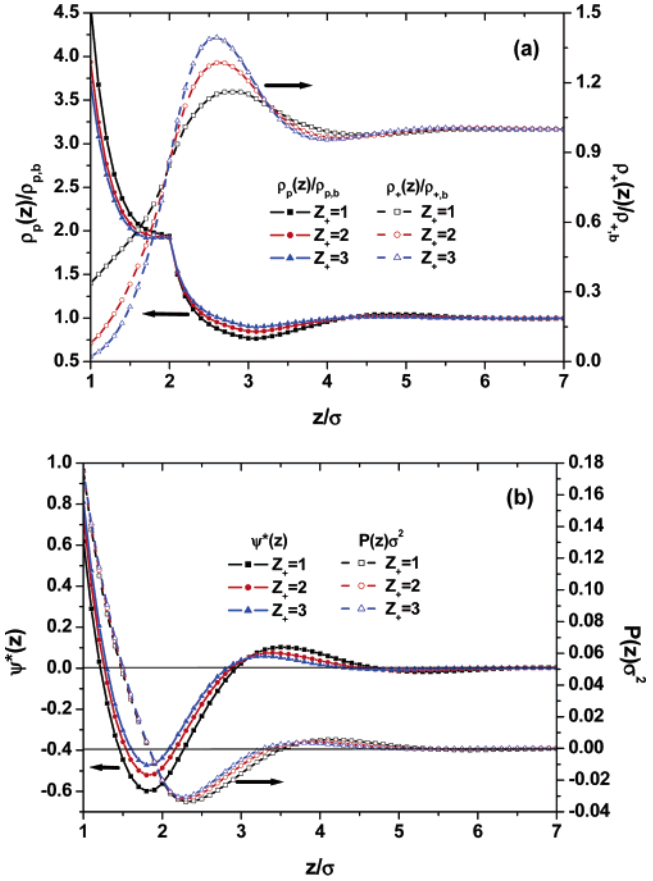

Figure 8. (a) Density distributions for polyions and counterions and (b) mean electrostatic potential profiles and integrated charge distribution functions at $Z_+ = 1$, 2, and 3. Here, $\rho_{p,b}\sigma_p^3 = 0.1$, $Q\sigma^2/e = 0.175$, $\sigma_p = \sigma_+ = \sigma = 0.425$ nm, $Z_p = -1$, and $M = 100$.

is due to the surface charge inversion or overcharging, as depicted in Figure 8b for the mean electrostatic potentials and integrated charge distribution functions. When the counterion valence increases, the absolute value of the minimum mean electrostatic potential and the magnitude of overcharging are slightly reduced due to the increased attraction of counterions in the bulk solution. Approximately, the minimum value of the electrostatic potential coincides with the position at the secondary layer of polyions, and a similar coincidence is observed between the minimum value of the integrated charge distribution function and the first peak in the density profile of counterions. As for the distribution of polyion segments, the counterion valence hardly affects the mean electrostatic potential or the integrated charge distribution.

To examine the effect of size disparity between polyion segments and counterions on polyelectrolyte adsorption, we present in Figure 9 the density profiles, electrostatic potentials, and integrated charge distributions for polyions with two segment diameters, $\sigma_p = 0.425$ and 0.85 nm. In both cases, the counterions are monovalent ($Z_+ = 1$) with the diameter $\sigma_+ = 0.425$ nm and the polyion length is $M = 20$. All other parameters are the same as those discussed in Figure 8. Figure 9a shows that, at the positively charged surface, the normalized polyion density is increased by nearly 8-fold as the segment size is doubled. The drastic increase in the relative polyion density can be explained by the fact that the number density at contact is primarily determined by the surface charge density while, at a fixed reduced density $\rho_{p,b}\sigma_p^3$, the number density in the bulk is proportional to σ_p^{-3}. As expected, the position of the secondary layer of polyions is directly related to the segment size and the

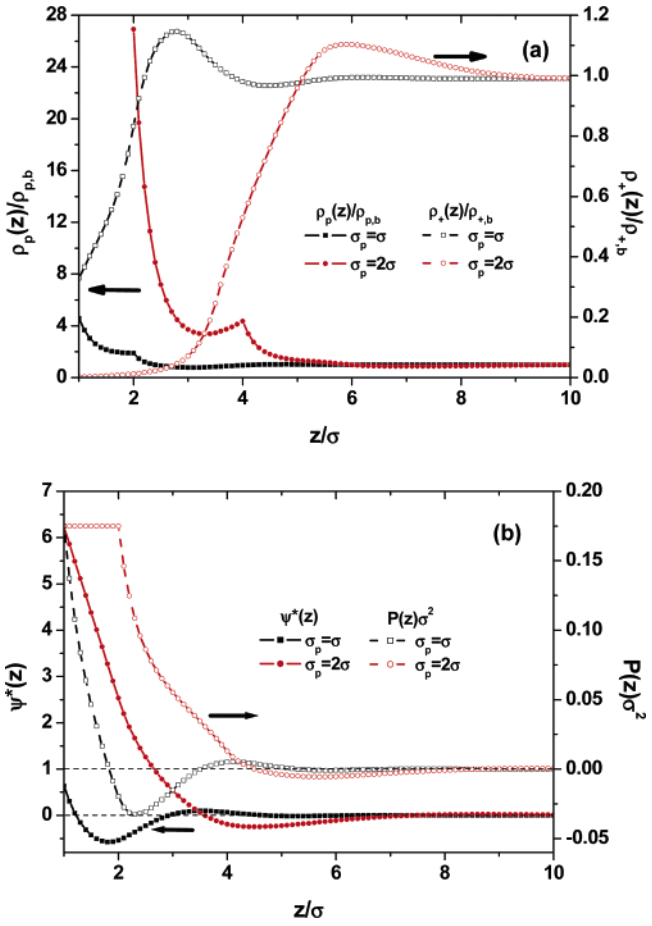

Figure 9. (a) Density distributions for polyions and counterions and (b) mean electrostatic potentials and integrated charge distribution functions for different diameters of polyion segments, $\sigma_p = \sigma$ and $\sigma_p = 2\sigma$. Except for the chain length and counterion valence (here $M = 20$ and $Z_+ = 1$), all parameters are the same as those used in Figure 8.

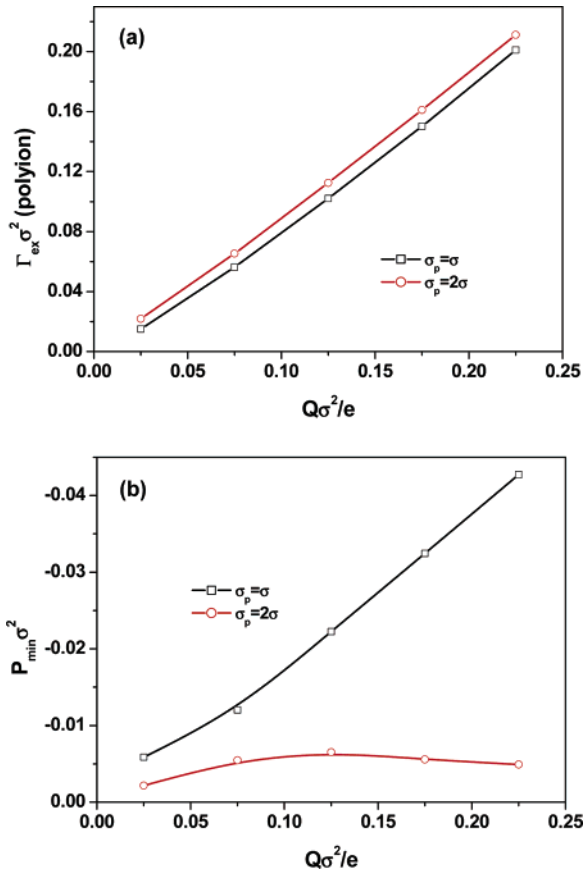

Figure 10. (a) Reduced surface excess of polyions and (b) minimum value of the integrated charge distribution function versus the surface charge density. All parameters are the same as those used in Figure 9.

counterions are distributed beyond the secondary polyion layer because of the electrostatic repulsion from the surface. Figure 9b shows the distributions of the mean electrostatic potentials and integrated charge distribution functions. Doubling the polyion size substantially reduces the magnitude of mean electrostatic potential at the position of the secondary layer of polyions and thereby makes the charge inversion less distinctive. For $\sigma_p = 0.85$ nm, the region $\sigma < z < 2\sigma$ is essentially inaccessible to both counterions and polyions so that, in this region, the integrated charge distribution function shows little change and the electrostatic potential decreases linearly away from the surface. The inaccessibility of polyions with $\sigma_p = 0.85$ nm at $z < 2\sigma$ also explains why the surface mean electrostatic potential for this case is much larger than that for $\sigma_p = 0.425$ nm.

Figure 10 parts a and b show, respectively, the reduced surface excesses of polyions and the minimum values of the integrated charge distribution functions versus the surface charge density at different values of the polyion segment diameter. Figure 10a indicates that the number of polyions adsorbed at the surface is proportional to the surface charge density and is little affected by the size of the polyion segments. This suggests that the adsorption of polyions is primarily determined by the direct electrostatic attraction between the polyions and surface charge. For polyions with $\sigma_p = 0.425$ nm, the minimum value of the integrated charge distribution function, or equivalently the magnitude of overcharging, rises sharply with the surface charge density. For polyions with larger segments, on the other hand, the magnitude of overcharging shows a weak maximum at an intermediate value of the surface charge density. In this case, the overcharging is restricted at high surface charge density probably due to the limitation of the maximum polyion packing density near the surface.

C. Electric Double Layers of Simple Electrolytes and of Polyelectrolytes. The DFT presented in this work allows us to investigate the structures of electric double layers for both simple and polyelectrolytes in a self-consistent manner. The numerical performance of the DFT for simple electrolytes has been demonstrated in our previous publications.[56−58] The results are akin to those shown in Figures 2−4 for polyelectrolytes. Comparison has also been made in our previous publications with the GC theory, modified PB equation (MPB), and alternative versions of DFT from the literature for simple electric double layers.[56−58] Figure 11 shows a further comparison of the density distributions of cations and anions near a negatively charged surface emerged in 2:1 and 2:2 electrolytes predicted by the DFT with the simulation results.

In Figures 12−14, we present the density profiles, electrostatic potentials, surface excesses, and integrated charge distributions for polyelectrolytes near an oppositely charged surface by varying the polyion chain length. As before, all systems are under salt-free conditions; i.e., there are no coions in the bulk solution. In these calculations, the segment diameter and reduced polyion density in the bulk are fixed at $\sigma_p = 0.425$ nm and $\rho_{p,b}\sigma_p^3 = 0.1$, respectively. Except for those specifically mentioned, all counterions bear one unit charge ($Z_+ = 1$) with diameter $\sigma_+ = 0.425$ nm. Figure 12a shows the density distributions of polyions and counterions of different chain

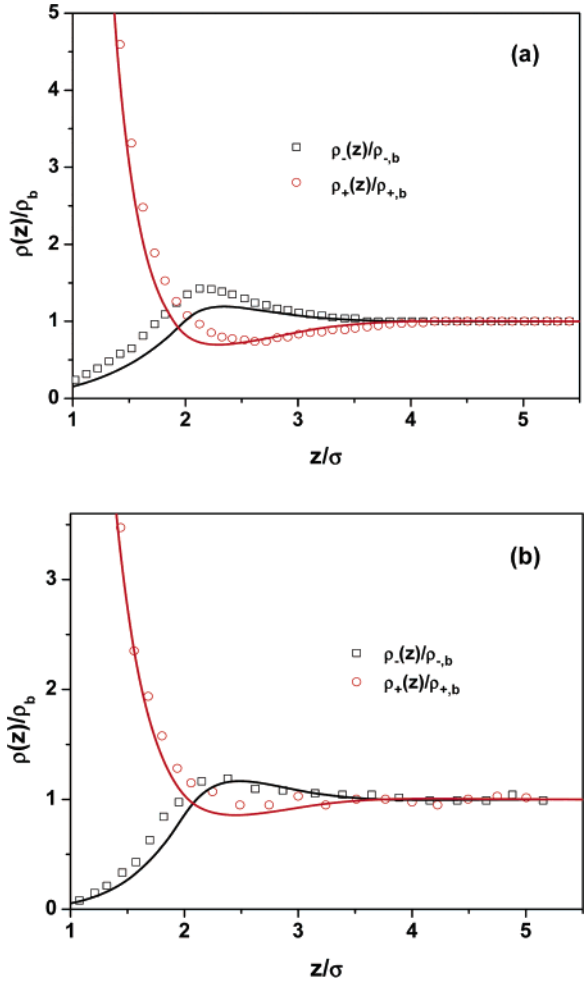

Figure 11. Density distributions for cations and anions in a simple electrolyte near a negatively charged surface: (a) 2:1, $\sigma_+ = \sigma_- = \sigma = 0.3$ nm, $Q\sigma^2/e = -0.1685$, $C = 1$mol/L; (b) 2:2, $\sigma_+ = \sigma_- = \sigma = 0.425$ nm, $Q\sigma^2/e = -0.1704$, $C = 0.5$mol/L. The lines are predictions of DFT, and the symbols are simulation results from refs 46 and 75.

lengths near a surface with the reduced charge density $Q\sigma^2/e = 0.075$. The corresponding mean electrostatic potentials and integrated charge distribution functions are depicted in Figure 12b. While a close similarity between the density profiles for $M = 2$, 3, 5, and 50 is observed, the ionic density profiles in the electric double layer of simple electrolytes ($M = 1$) is noticeably different from those for polyions. Near the weakly charged surface, the contact density of monomeric ions is much larger than that of polyions due to the restriction of the polymer degree of freedom by the surface. However, a secondary peak is absent in the density profile of monomeric ions. In addition, in contrast to that for polyions, the density profile for $M = 1$ does not exhibit much oscillation beyond $z/\sigma > 2$. The remarkable difference between the density profiles of monomeric ions and polyions suggests that the layering structure of polyions near an oppositely charged surface arises not only from the excluded-volume effects of polymer segments but also from the chain connectivity. For $M = 1$, the mean electric potential at the surface is significantly lower than those for polyions, suggesting that monomeric ions neutralize the weakly charged surface more efficiently than polyions. However, no significant charge inversion is observed for monomeric ions probably due to the weak charge correlations at the surface.

Figure 13a presents the contact values of the mean electrostatic potential versus the surface charge density for simple

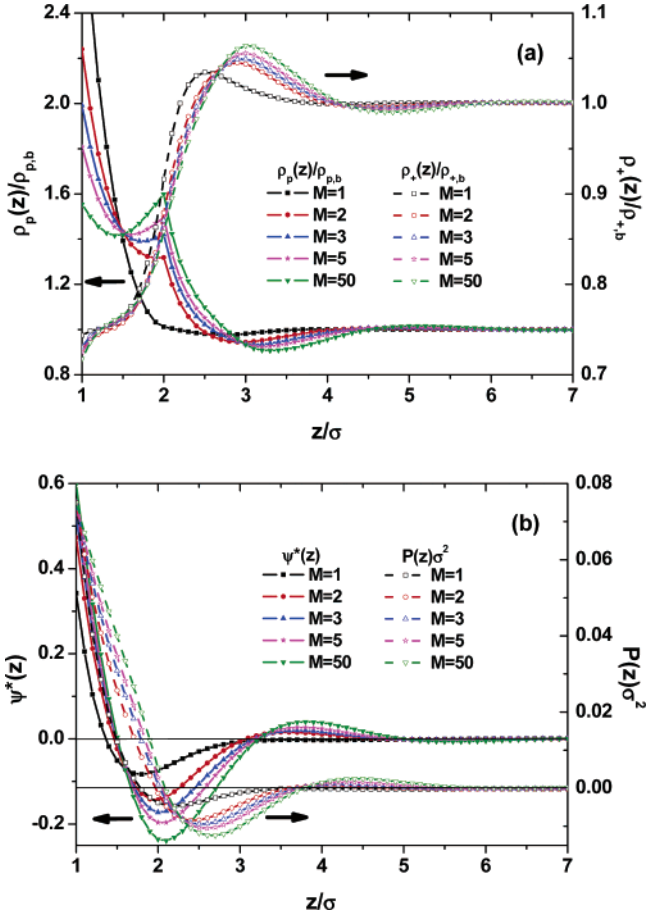

Figure 12. (a) Density distributions for polyions and small cations and (b) mean electrostatic potentials and integrated charge distribution functions for $M = 1$, 2, 3, 5, and 50. Here, $\rho_{p,b}\sigma_p^3 = 0.1$, $Q\sigma^2/e = 0.075$, $\sigma_p = \sigma_+ = \sigma = 0.425$ nm, and $Z_p = -Z_+ = -1$.

electrolytes ($M = 1$) and for polyelectrolytes ($M = 100$) at three valences of counterions. For simple electrolytes, the contact potential is approximately a linear function of the surface charge density. For polyions, however, the contact potential is relatively insensitive to the surface charge density, and for monovalent counterions, it shows a weak maximum at an intermediate value of the surface charge density. Near a weakly charged surface, the contact electrostatic potential in the presence of simple electrolytes is significantly lower than that in the presence of polyions, whereas the opposite is true at a strongly charged surface where the direct Coulomb interactions overrule the steric effects. In the latter case, the adsorption of polyanions in the vicinity of the surface is stronger than that of simple anions. At low surface charge density, the contact potentials for both monomeric ions and polyions decrease with the increase of the counterion valence but the trend is reversed at high surface charge density. Figure 13b shows the surface excesses versus the surface charge density at different chain lengths ($Z_+ = 1$). As suggested by Figure 13a, the adsorption of polyanions near a weakly charged surface is less favorable than that of simple anions owing to the entropy-driven depletion but the trend is again opposite near a strongly charged surface where the electrostatic attraction from the surface suppresses the steric effects. Because the adsorption of polyions is mainly determined by charge neutralization, the extent of charge inversion is fairly small in comparison to the surface charge and the surface excess appears insensitive to the polyion chain length.

Figure 14 shows the contact and minimum values of the mean electrostatic potential as a function of the polyion chain length

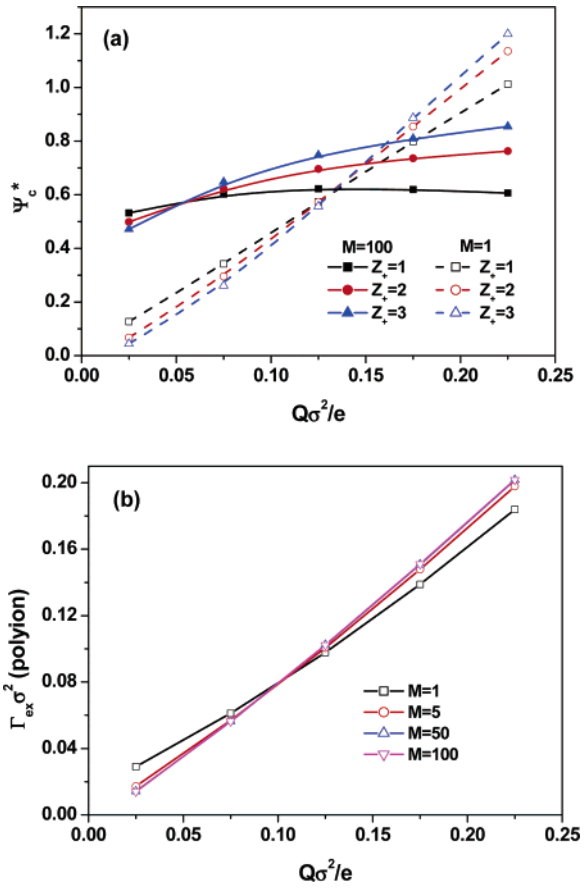

Figure 13. (a) Contact value of the mean electrostatic potential versus the surface charge density for simple ($M = 1$) and polyelectrolyte ($M = 100$) at different valences of counterions ($Z_+ = 1$, 2, and 3). (b) Surface excess versus the surface charge density for $M = 1$, 5, 50, and 100 and $Z_+ = 1$. In both cases, $\rho_{p,b}\sigma_p^3 = 0.1$, $\sigma_p = \sigma_+ = \sigma = 0.425$ nm, and $Z_p = -1$.

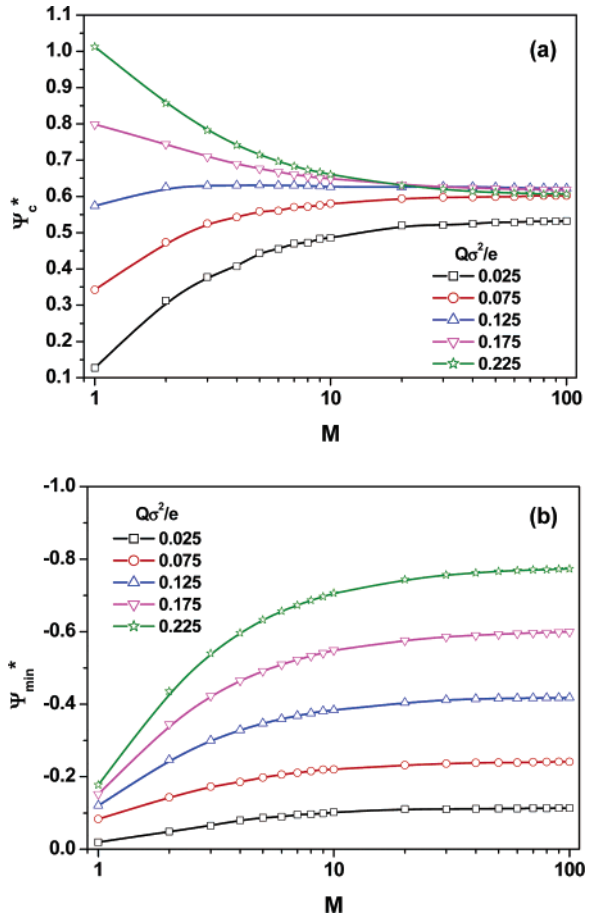

Figure 14. (a) Contact and (b) minimum values of the mean electrostatic potential versus the polyion chain length at different surface charge densities. Here, $\rho_{p,b}\sigma_p^3 = 0.1$, $\sigma_p = \sigma_+ = \sigma = 0.425$ nm, and $Z_p = -Z_+ = -1$.

at five different surface charge densities. Near a weakly charged surface, the contact potential monotonically increases with the polyion chain length due to the increased steric interactions. At a highly charged surface, on the other hand, the contact electrostatic potential falls as the chain length increases. In this case, the decrease in the contact potential is attributed to the charge correlations and to the direct electrostatic attraction from the surface. As discussed in Figure 13a, for polyions, the contact potential is relatively insensitive to the surface charge density, whereas, for simple electrolytes, it is approximately a linear function of the surface charge density. Figure 14b shows the effect of the chain length on the magnitude of charge inversion as represented by the minimum value of the mean electrostatic potential. It indicates that charge inversion becomes more prominent as the polyion chain length increases. Because the minimum electrostatic potential appears at approximately 2σ, a close inspection of the density profiles of both polyions and counterions near the surface reveals that the influence of chain length on the adsorption varies with the surface charge density. When $Q\sigma^2/e = 0.025$, the adsorption for both polyions and counterions decreases with the chain length but a more pronounced influence is observed for counterions. When $Q\sigma^2/e = 0.075$, the adsorption for polyions increases but for counterions it decreases with the chain length. When $Q\sigma^2/e > 0.075$, however, the adsorption for both polyions and counterions increases with the chain length but for polyions it increases more rapidly. Figure 14b also shows that the effect of the surface charge density on the magnitude of charge inversion becomes stronger as the polyion chain length increases.

IV. Conclusions

We have introduced a nonlocal density functional theory (NLDFT) for polyelectrolyte solutions within the primitive model by extending our previous work for simple electrolytes and polymers. The numerical performance of the NLDFT has been successfully tested with simulation results from the literature for the density distributions of polyion segments and small ions and for the surface excesses of polyions at different solution concentrations and surface charge densities. The theory faithfully captures the charge inversion and layering effects that are not reproduced by previous theories of polyelectrolyte solutions.

We have also elucidated the influences of small ion valence, polyion chain length, and size disparity between polyion segments and small ions on the microscopic structure, mean electrostatic potential, and overcharging for polyelectrolytes in contact with an oppositely charged surface. It is found that the adsorption of polyelectrolytes is mainly determined by the electrostatic neutralization of the surface and varies little with the counterion size and valence, the diameter of polyion segments, or the polyion chain length. Even for polyions with a chain length up to $M = 100$, the segmental density profile shows little long-range correlations in the direction perpendicular to the surface, suggesting that the effects of the chain connectivity and electrostatic correlations are substantially sup-

pressed by the direct Coulomb attraction from the surface. Whereas for simple electrolytes the contact potential of an electric double layer depends almost linearly on the surface charge density, in the presence of polyions, the contact potential is relatively insensitive to the surface charge density or the valence of small ions.

The charge inversion and overcharging are manifested in the distribution of the mean electrostatic potential and in the integrated charge distribution function, respectively. For polyions near an oppositely charged surface, the minimum value of the electrostatic potential approximately coincides with the position at the secondary layer of polyions and a similar coincidence exists between the minimum value of the integrated charge distribution function and the first peak in the density profile of counterions. The layering structure of polyions and oscillation of small ion distributions are not shown in a previous version of DFT or alternative methods based on the PB equation. As the counterion valence increases, the magnitude of charge inversion is slightly reduced due to the increased attraction of counterions in the bulk solution. The charge inversion and overcharging are also weakened by increasing the size of the polymer segments but become more prominent as the polyion chain length or the surface charge density increases. Near a weakly charged positive surface, the contact density of monomeric anions is much larger than that of polymeric anions due to the restriction of the polymer configurations, and the contact value of the electrostatic potential in the presence of simple electrolytes is significantly lower than that in the presence of polyions. In this case, the contact potential decreases with the counterion valence but increases with the polyion chain length. Near a highly charged surface, on the other hand, the contact value of the electrostatic potential falls as the chain length increases. In that case, the adsorption of polymeric anions is favored over monomeric anions and the surface potential increases with the valence of small ions.

Although this work is only concerned with polyelectrolytes near an oppositely charged surface, the DFT is equally applicable to polyions near a surface of like charge or to block copolymers of mixed charge status for individual segments. By considering the two-dimensional inhomogeneity of the system, we may also investigate the orientation of polyion distributions, i.e., whether the polyions are parallel or perpendicular to the surface. While the overall performance of the NLDFT is satisfactory in comparison with simulations, its application to experimental systems is still limited by the primitive model that retains only the essential features of electrostatic interactions. Besides, the NLDFT also overpredicts the polyion densities near a weakly charged surface. To provide a more realistic representation of polyelectrolyte solutions, we need to consider also van der Waals attractions among polymer segments, counterions, and the external surface that may have significant effects on the adsorption behavior. Furthermore, the numerical performance of the NLDFT can be improved by incorporation of multibody cavity correlation functions into the Helmholtz energy functional for chain connectivity. Work along these directions is in progress.

Acknowledgment. The authors are grateful to Arun Yethiraj and Chandra N. Patra for providing the simulation data prior to publication. This work is financially supported by the National Science Foundation (CTS0406100 and CTS0340948).

Appendix

The grand potential and Helmholtz energy functional are connected by the Legend transformation

$$\Omega[\rho_M(\mathbf{R}),\{\rho_\alpha(\mathbf{r})\}] = F[\rho_M(\mathbf{R}),\{\rho_\alpha(\mathbf{r})\}] + \int[\Psi_M(\mathbf{R}) - \mu_M]\rho_M(\mathbf{R})\,d\mathbf{R} + \sum_{\alpha=+,-}\int d\mathbf{r}\,\rho_\alpha(\mathbf{r})[\Psi_\alpha(\mathbf{r}) - \mu_\alpha] \quad \text{(A1)}$$

where $d\mathbf{R} = d\mathbf{r}_1, d\mathbf{r}_2, ..., d\mathbf{r}_M$ represents a set of differential volumes, $\rho_M(\mathbf{R})$ stands for a multidimensional polyion density profile as a function of the polymer configuration $\mathbf{R}$, $\rho_\alpha(\mathbf{r})$ is the density profiles of small ions, and μ_M and μ_α are, respectively, the chemical potentials of the polyions and small ions. For polyelectrolyte solutions considered in this work, the external potential $\Psi_M(\mathbf{R})$ applies to individual segments of polyions; i.e.,$\Psi_M(\mathbf{R}) = \sum_{i=1}^{M}\Psi_p(\mathbf{r}_i)$. $\Psi_\alpha(\mathbf{r})$ is the external potential for small ions.

In general, the Helmholtz energy functional includes an ideal-gas term that depends on the bond potentials and molecular architecture and an excess term accounting for various contributions due to the nonbonded interactions leading to the thermodynamic nonideality. Within the framework of the primitive model, the Helmholtz energy functional of a polyelectrolyte solution can be decomposed into five contributions, i.e.,

$$F = F^{id} + F_{hs}^{ex} + F_{ch}^{ex} + F_C^{ex} + F_{el}^{ex} \quad \text{(A2)}$$

where F^{id} is the intrinsic Helmholtz energy functional for an ideal gas that is free of nonbonded interactions, F_{hs}^{ex} represents the contribution to the excess Helmholtz energy functional due to hard-sphere repulsions, F_{ch}^{ex} is that due to the effect of chain connectivity on intramolecular correlations, F_C^{ex} represents the direct Coulomb energy, and F_{el}^{ex} is the excess Helmholtz energy functional arising from the electrostatic correlations.

The ideal-gas term F^{id} is known exactly; it depends on the polyion configurations, the bond potential $V_b(\mathbf{R})$, and the density profiles of small ions:

$$\beta F^{id} = \int d\mathbf{R}\,\rho_M(\mathbf{R})[\ln\rho_M(\mathbf{R}) - 1] + \beta\int d\mathbf{R}\,\rho_M(\mathbf{R})V_b(\mathbf{R}) + \sum_{\alpha=+,-}\int d\mathbf{r}\,\rho_\alpha(\mathbf{r})[\ln\rho_\alpha(\mathbf{r}) - 1] \quad \text{(A3)}$$

The excess Helmholtz energy functional due to the hard-sphere repulsion, F_{hs}^{ex}, can be accurately described by a modified fundamental measure theory (MFMT)[59,60]

$$\beta F_{hs}^{ex} = \int \Phi^{hs}[n_\omega(\mathbf{r})]\,d\mathbf{r} \quad \text{(A4)}$$

in which the reduced excess energy density Φ^{hs} is a function of six weighted densities $n_\omega(\mathbf{r})$[72]

$$\Phi^{hs} = -n_0\ln(1-n_3) + \frac{n_1n_2 - \mathbf{n}_{V1}\mathbf{n}_{V2}}{1-n_3} + \frac{1}{36\pi}\left[n_3\ln(1-n_3) + \frac{n_3^2}{(1-n_3)^2}\right]\frac{(n_2^3 - 3n_2\mathbf{n}_{V2}\mathbf{n}_{V2})}{n_3^3} \quad \text{(A5)}$$

According to an extension of the first-order thermodynamic perturbation theory (TPT1),[66] the excess Helmholtz energy functional for chain connectivity F_{ch}^{ex} can also be expressed in terms of the weighted densities

$$\beta F_{ch}^{ex} = \frac{1-M}{M}\int n_{0p}\zeta_p\ln y(\sigma_p,n_\omega)\,d\mathbf{r} \quad \text{(A6)}$$

where $\zeta_p = 1 - \mathbf{n}_{V2p}\mathbf{n}_{V2p}/n_{2p}^2$, and $y(\sigma_p,n_\omega)$ stands for the contact value of the cavity correlation function (CCF) of the polymer

segments when they are disconnected (i.e., in a solution of monomeric charged spheres)[39,73]

$$y(\sigma_p,n_\omega)=\left[\frac{1}{1-n_3}+\frac{n_2\sigma_p(1-\mathbf{n}_{V2}\mathbf{n}_{V2}/n_2^2)}{4(1-n_3)^2}\right]\times \exp\left(-\frac{\Gamma^2 a_p^2}{4\pi^2 l_B\sigma_p}\right)\exp\left(\frac{l_B Z_p^2}{\sigma_p}\right) \quad (A7)$$

Similar to the thermodynamic perturbation theory of bulk polyelectrolyte solutions,[39,73] the parameters Γ and a_p can be calculated from

$$\Gamma=\sqrt{\pi l_B\sum_{k=p,+,-}n_{0k}\left(\frac{1}{1+\Gamma\sigma_k}\right)^2\left(Z_k-\frac{\pi P_n\sigma_k^2}{2(1-n_3)}\right)^2} \quad (A8)$$

$$a_p=\frac{2\pi l_B\left(Z_p-\frac{\pi P_n\sigma_p^2}{2(1-n_3)}\right)}{\Gamma(1+\Gamma\sigma_p)} \quad (A9)$$

with

$$P_n=\sum_{k=p,+,-}\frac{2n_{1k}Z_k}{1+\Gamma\sigma_k}\Big/\left(1+\frac{3}{(1-n_3)}\sum_{k=p,+,-}\frac{n_{3k}}{1+\Gamma\sigma_k}\right) \quad (A10)$$

Finally, the Helmholtz energy due to the Coulomb interactions include two parts: one is the direct Coulomb interaction as it appeared in the PB equation and the second part accounts for the correlation of charge distributions. The direct Coulomb term F_C^{ex} is known exactly

$$\beta F_C^{ex}=\frac{l_B}{2}\sum_{i,j=p,+,-}\int\int d\mathbf{r}\,d\mathbf{r}'\frac{Z_iZ_j\rho_i(\mathbf{r})\,\rho_j(\mathbf{r}')}{|\mathbf{r}-\mathbf{r}'|} \quad (A11)$$

Conversely, the Helmholtz energy functional F_{el}^{ex} due to the electrostatic correlations can be approximated by a quadratic functional Taylor expansion with respect to that for a monomeric bulk fluid of densities $\{\rho_i^b\}$[56,57]

$$\beta F_{el}^{ex}=\beta F_{el}^{ex}[\{\rho_i^b\}]-\int d\mathbf{r}\sum_{i=p,+,-}\Delta C_i^{(1)el}(\rho_i(\mathbf{r})-\rho_i^b)-\frac{1}{2}\int\int d\mathbf{r}\,d\mathbf{r}'\sum_{i,j=p,+,-}\Delta C_{ij}^{(2)el}(|\mathbf{r}-\mathbf{r}'|)(\rho_i(\mathbf{r})-\rho_i^b)(\rho_j(\mathbf{r}')-\rho_j^b) \quad (A12)$$

where the residual first-order and second-order direct correlation functions (DCF) are defined as, respectively,

$$\Delta C_i^{(1)el}=-\beta\mu_i^{el}=-\delta\beta F_{el}^{ex}/\delta\rho_i(\mathbf{r})|_b \quad (A13)$$

$$\Delta C_{ij}^{(2)el}(|\mathbf{r}-\mathbf{r}'|)=-\delta^2\beta F_{el}^{ex}/\delta\rho_i(\mathbf{r})\delta\rho_j(\mathbf{r}')|_b \quad (A14)$$

In writing eq A12, we have assumed that the effect of chain connectivity on the electrostatic part of the direct correlation functions can be neglected. With this assumption, $\Delta C_{ij}^{(2)el}(r)$ can be obtained from the mean-spherical approximation (MSA) for simple electrolytes[69,74]

$$\Delta C_{ij}^{(2)el}(r)=C_{ij}(r)+\frac{l_BZ_iZ_j}{r}-C_{ij}^{hs}(r) \quad (A15)$$

Conceivably, alternative methods, such as a more accurate theory of electrolyte solutions, can also be used to calculate $\Delta C_{ij}^{(2)el}(r)$.

For polyelectrolytes near a uniformly charged planar surface, the density profiles of polyions and small ions vary only in the z direction. In this case, the density profiles for small ions and polyions are given by, respectively

$$\rho_\alpha(z)=\exp\left[\beta\mu_\alpha-\beta\Psi_\alpha(z)-\frac{\delta\beta F^{ex}}{\delta\rho_\alpha(z)}\right] \quad (A16)$$

$$\rho_p(z)=\exp(\beta\mu_M)\sum_{i=1}^{M}\exp[-\beta\lambda_p(z)]G^i(z)G^{M+1-i}(z) \quad (A17)$$

with $\lambda_p(z)=\delta F_{ex}/\delta\rho_p(z)+\Psi_p(z)$. The propagator function $G^i(z)$ is determined from the recurrence relation

$$G^i(z)=\int dz'\exp[-\beta\lambda_p(z')]\frac{\theta(\sigma_p-|z-z'|)}{2\sigma_p}G^{i-1}(z') \quad (A18)$$

for $i=2,\ldots,M$ with $G^1(z)=1$. The mean electrostatic potential $\psi(\mathbf{r})$ is given by

$$\psi^*(z)\equiv\beta e\psi(z)=4\pi l_B\int_z^\infty dz'\,(z-z')\sum_{k=p,+,-}Z_k\rho_k(z') \quad (A19)$$

Equation A19 is derived from the integration of the Poisson equation with the boundary conditions $d\psi(z)/dz|_{z=\infty}=0$ and $\psi(z=\infty)=0$. For computational convenience, it can be expressed as

$$\psi^*(z)=\psi^*(z=0)+4\pi l_B\left[\int_z^\infty dz'\,z\sum_{k=p,+,-}Z_k\rho_k(z')+\int_0^z dz'\,z'\sum_{k=p,+,-}Z_k\rho_k(z')\right] \quad (A20)$$

The density distributions of polyion segments, cations, and anions satisfy the electroneutrality condition

$$\int_0^\infty dz'\sum_{k=p,+,-}Z_ke\rho_k(z')+Q=0 \quad (A21)$$

The Picard iteration is applied to solve eqs A16 and A17. The iteration starts with the bulk densities for the density profiles of polyion segments and small ions. The effective fields $\delta F_{ex}/\delta\rho_k(z)+\Psi_k(z)$ and the function $G^i(z)$ are then calculated, and subsequently, a set of new density profiles are calculated from eqs A16 and A17. The calculated density profiles are mixed with the previous results as the new inputs. The iteration repeats until the change between normalized densities of the input and the output at all positions is smaller than 0.1%.

References and Notes

(1) Levin, Y. *Rep. Prog. Phys.* **2002**, *65*, 1577.
(2) Naji, A.; Jungblut, S.; Moreira, A. G.; Netz, R. R. *Physica A* **2005**, *352*, 131.
(3) Holm, C.; Joanny, J. F.; Kremer, K.; Netz, R. R.; Reineker, P.; Seidel, C.; Vilgis, T. A.; Winkler, R. G. *Adv. Polym. Sci.* **2004**, *166*, 67.
(4) Boroudjerdi, H.; Netz, R. R. *J. Phys.: Condens. Matter* **2005**, *17*, S1137.
(5) Gouy, G. *J. Phys. Radium* **1910**, *9*, 457.
(6) Chapman, D. L. *Philos. Mag.* **1913**, *25*, 475.
(7) Debye, P.; Huckel, E. *Phys. Z.* **1923**, *24*, 185.
(8) Robinson, R. A.; Stokes, R. H. *Electrolyte Solutions*, 2nd ed.; Butterworth: London, 1970.
(9) *Activity coefficients in electrolyte solutions*; Pitzer, K. S., Ed.; CRC Press: Boca Raton, FL, 1991.

(10) Loehe, J. R.; Donohue, M. D. *AIChE J.* **1997**, *43*, 180.
(11) Wu, J. Z.; Prausnitz, J. M. *Ind. Eng. Chem. Res.* **1998**, *37*, 1634.
(12) Varela, L. M.; Garcia, M.; Mosquera, V. *Phys. Rep.* (review section of *Phys. Lett.*) **2003**, *382*, 1.
(13) Rasaiah, J. C.; Friedman, H. L. *J. Chem. Phys.* **1968**, *48*, 2742.
(14) Waisman, E.; Lebowitz, J. L. *J. Chem. Phys.* **1970**, *52*, 4307.
(15) Blum, L. *Mol. Phys.* **1975**, *35*, 299.
(16) Hoye, J. S.; Stell, G. *J. Chem. Phys.* **1977**, *67*, 439.
(17) Outhwaite, C. W. *J. Chem. Soc., Faraday Trans. 2* **1978**, *74*, 1214.
(18) Torrie, G. M.; Valleau, J. P.; Patey, G. N. *J. Chem. Phys.* **1982**, *76*, 4615.
(19) Carnie, S. L.; Torrie, G. M. *Adv. Chem. Phys.* **1984**, *56*, 141.
(20) Wu, J. Z.; Lu, J. F.; Li, Y. G. *Fluid Phase Equilib.* **1994**, *101*, 121.
(21) Katchalsky, A. *Pure Appl. Chem.* **1971**, *26*, 327.
(22) Manning, G. S. *J. Chem. Phys.* **1967**, *47*, 2010.
(23) Gueron, M.; Weisbuch, G. *J. Phys. Chem.* **1979**, *83*, 1991.
(24) van den Hoop, M. A. G. T.; Porasso, R. D.; Benegas, J. C. *Colloids Surf., A* **2002**, *203*, 105.
(25) Labarbe, R.; Flock, S.; Maus, C.; Houssier, C. *Biochemistry* **1996**, *35*, 3319.
(26) Korolev, N.; Lyubartsev, A. P.; Nordenskiold, L. *Biophys. J.* **1998**, *75*, 3041.
(27) Record, M. T.; Lohman, T. M. *Biopolymers* **1978**, *17*, 159.
(28) Barrat, J. L.; Joanny, J. F. *Adv. Chem. Phys.* **1996**, *94*, 1.
(29) Netz, R. R.; Andelman, D. *Phys. Rep.* (review section of *Phys. Lett.*) **2003**, *380*, 1.
(30) Podgornik, R. *J. Phys. Chem.* **1992**, *96*, 884.
(31) Muthukumar, M. *J. Chem. Phys.* **1987**, *86*, 7230.
(32) Vilgis, T. A.; Borsali, R. *Phys. Rev. A* **1991**, *43*, 6857.
(33) Zhulina, E. B.; Wolterink, J. K.; Borisov, O. V. *Macromolecules* **2000**, *33*, 4945.
(34) Wang, Q.; Taniguchi, T.; Fredrickson, G. H. *J. Phys. Chem. B* **2004**, *108*, 6733.
(35) Huang, H. H.; Ruckenstein, E. *Adv. Colloid Interface Sci.* **2004**, *112*, 37.
(36) Akesson, T.; Woodward, C.; Jonsson, B. *J. Chem. Phys.* **1989**, *91*, 2461.
(37) Yethiraj, A.; Shew, C. Y. *Phys. Rev. Lett.* **1996**, *77*, 3937.
(38) von Solms, N.; Chiew, Y. C. *J. Chem. Phys.* **1999**, *111*, 4839.
(39) Jiang, J. W.; Liu, H. L.; Hu, Y.; Prausnitz, J. M. *J. Chem. Phys.* **1998**, *108*, 780.
(40) Evans, R. Density functionals in the theory of nonuniform fluids. In *Fundamentals of Inhomogeneous Fluids*; Henderson, D., Ed.; Marcel Dekker: New York, 1992; p 85.
(41) Wu, J. Z. *AIChE J.* **2005**, in press.
(42) Stevens, M. J.; Robbins, M. O. *Europhys. Lett.* **1990**, *12*, 81.
(43) Tang, Z. X.; Scriven, L. E.; Davis, H. T. *J. Chem. Phys.* **1991**, *95*, 2659.
(44) Hansen, J. P.; Lowen, H. *Annu. Rev. of Phys. Chem.* **2000**, *51*, 209.
(45) Henderson, D.; Bryk, P.; Sokolowski, S.; Wasan, D. T. *Phys. Rev. E* **2000**, *61*, 3896.
(46) Boda, D.; Fawcett, W. R.; Henderson, D.; Sokolowski, S. *J. Chem. Phys.* **2002**, *116*, 7170.
(47) Patra, C. N.; Ghosh, S. K. *J. Chem. Phys.* **2002**, *117*, 8938.
(48) Bhuiyan, L. B.; Outhwaite, C. W. *Phys. Chem. Chem. Phys.* **2004**, *6*, 3467.
(49) vanRoij, R.; Hansen, J. P. *Phys. Rev. Lett.* **1997**, *79*, 3082.
(50) Gillespie, D.; Nonner, W.; Eisenberg, R. S. *Phys. Rev. E* **2003**, *68*, Article No. 031503.
(51) Chan, D. Y. C. *Phys. Rev. E* **2001**, *63*, 061806.
(52) Patra, C. N.; Chang, R.; Yethiraj, A. *J. Phys. Chem. B* **2004**, *108*, 9126.
(53) Bryk, P. *J. Chem. Phys.* **2005**, *122*, 174906.
(54) Li, Z. D.; Wu, J. Z. *Phys. Rev. E* **2004**, *70*, 031109.
(55) Li, Z. D.; Wu, J. Z. *Macromol. Symp.* **2005**, *219*, 51.
(56) Yu, Y. X.; Wu, J. Z.; Gao, G. H. *J. Chem. Phys.* **2004**, *120*, 7223.
(57) Wang, K.; Yu, Y. X.; Gao, G. H. *Phys. Rev. E* **2004**, *70*, 011912.
(58) Yu, Y. X.; Wu, J. Z.; Gao, G. H. *Chin. J. Chem. Eng.* **2004**, *12*, 688.
(59) Roth, R.; Evans, R.; Lang, A.; Kahl, G. *J. Phys.: Condens. Matter* **2002**, *14*, 12063.
(60) Yu, Y. X.; Wu, J. Z. *J. Chem. Phys.* **2002**, *117*, 10156.
(61) Patra, C. N.; Ghosh, S. K. *J. Chem. Phys.* **1994**, *101*, 4143.
(62) Patra, C. N.; Ghosh, S. K. *J. Chem. Phys.* **1994**, *100*, 5219.
(63) Patra, C. N.; Yethiraj, A. *J. Phys. Chem. B* **1999**, *103*, 6080.
(64) Mier-y-Teran, L.; Suh, S. H.; White, H. S.; Davis, H. T. *J. Chem. Phys.* **1990**, *92*, 5087.
(65) Kierlik, E.; Rosinberg, M. L. *J. Chem. Phys.* **1993**, *99*, 3950.
(66) Yu, Y. X.; Wu, J. Z. *J. Chem. Phys.* **2002**, *117*, 2368.
(67) Yethiraj, A.; Patra, C. N. Personal communications, 2005.
(68) Li, Z. D.; Wu, J. Z. *Phys. Rev. Lett.* **2006**, *96*, 048302.
(69) Blum, L. *Mol. Phys.* **1975**, *30*, 1529.
(70) Li, Z. D.; Cao, D. P.; Wu, J. Z. *J. Chem. Phys.* **2005**, *122*, 174708.
(71) Yu, Y. X.; Wu, J. Z. *J. Chem. Phys.* **2002**, *116*, 7094.
(72) Rosenfeld, Y. *Phys. Rev. Lett.* **1989**, *63*, 980.
(73) Jiang, J. W.; Blum, L.; Bernard, O.; Prausnitz, J. M. *Mol. Phys.* **2001**, *99*, 1121.
(74) Hoye, J. S.; Blum, L. *Mol. Phys.* **1978**, *35*, 299.
(75) Torrie, G. M.; Valleau, J. P. *J. Phys. Chem.* **1982**, *86*, 3251.